



ELSEVIER

Available online at www.sciencedirect.com

SCIENCE @ DIRECT®

Ocean Engineering 31 (2004) 1093–1109

OCEAN
ENGINEERING

www.elsevier.com/locate/oceaneng

Run-up heights of nearshore tsunamis based on quadtree grid system

Yong-Sik Cho^{a,*}, Koo-Yong Park^b, Tae-Hoon Lin^a

^a Department of Civil Engineering, Hanyang University, 17 Haengdang-dong, Seongdong-gu, Seoul 133-791, South Korea

^b Hyundai Engineering and Construction Co., 140-2 Kye-dong, Chongro-gu, Seoul 110-793, South Korea

Received 25 June 2003; accepted 22 October 2003

Abstract

To investigate the run-up heights of nearshore tsunamis in the vicinity of a circular island, a numerical model has been developed based on quadtree grids. The governing equations of the model are the nonlinear shallow-water equations. The governing equations are discretized explicitly by using the leap-frog scheme on adaptive hierarchical quadtree grids. The refined quadtree grids are generated around a circular island on a combined domain of rectangular and circular grids. The predicted numerical results have been verified by comparing to available laboratory measurements. A good agreement has been observed.

© 2004 Elsevier Ltd. All rights reserved.

Keywords: Quadtree; Nearshore tsunami; Run-up; Shallow-water equations; Circular island; Finite difference scheme

1. Introduction

Tsunamis are large water waves set in motion either by landslides, submarine volcanic explosions, or sea-bottom deformations associated with large submarine earthquakes. During the last decades several devastating tsunamis have occurred around the Pacific Ocean area (Gonzalez, 1999). These tsunamis not only killed many human beings but also caused serious property damages. Especially, near-shore tsunamis could cause severe coastal flooding and huge property damage; because it takes a few minutes to reach a coastline and the time to seek refuge from

* Corresponding author. Tel.: +82-2-2290-0393; fax: 82-2-2293-9977.
E-mail address: ysc59@hanyang.ac.kr (Y.-S. Cho).

Nomenclature

A	wave height of incident wave
D	base diameter of island
g	gravity acceleration
h	still-water depth
H	total water depth, $\zeta + h$
n	Manning's relative roughness coefficient
P, Q	Cartesian component of volume flux
R	run-up height
t	time
β	angle
λ	length of directional spectral wave generator
ε	nonlinearity of incident wave, A/h
τ_x, τ_y	bottom friction stress
ζ	free surface displacement

Subscripts

C	cell centre
E	east node
W	west node
S	south node
N	north node

a tsunami is not enough. The 1992 Flores tsunami killed more than 264 people in Indonesia and the 1993 Hokkaido tsunami in Japan killed 239 people and caused the huge run-up heights of Babi and Okushiri Islands, respectively (Liu et al., 1995). Therefore, a coastal inundation map based on the maximum run-up heights is essential to mitigate coastal casualties from unexpected nearshore tsunami attacks (Liu et al., 1995).

Pelinovsky et al. (1999) studied run-up of tsunamis on a vertical wall in a bay of different cross-section using shallow-water equations. However, the run-up heights should be evaluated on an inclined wall to make the inundation map. The solitary wave which is adopted in this paper is considered a valid representation of the tsunami (Silva et al., 2000) to present a reflection and transmission of tsunami waves by coastal structures.

In this paper, an adaptive quadtree grid system will be employed to investigate the run-up heights of nearshore tsunamis around a circular island. Based on the numerical model developed by Liu et al. (1995), the maximum run-up heights of tsunami attacking a circular island will be re-calculated. The adaptive hierarchical quadtree grids will be generated around a circular island. The uniformed rectangular meshes provided by Liu et al. will be used out of the island, while a localized

high resolution meshes will be adapted around boundaries of the island with the rectangular and circular domains. The newly obtained maximum run-up heights will be compared with those of Liu et al. and laboratory measurements done at the Coastal Engineering Research Center (CERC), US Army Corps of Engineers (Liu et al., 1995; Cho and Liu, 1999).

A brief description of laboratory facility will firstly be introduced for completeness in the paper. The governing equations will be discretized with a finite difference scheme on the adapted quadtree grids. Particular attention will be paid to validating the computational results with Liu et al.'s numerical solutions, the quadtree grid method and experimental measurements for the maximum run-up heights of nearshore tsunami around a circular island. Finally, careful discussion on the numerical solutions and concluding remarks will be described.

2. Laboratory experiments

Laboratory experiments were performed in a large scale basin at the CERC. The basin was 30 m wide and 25 m long as shown in Fig. 1. The center of a circular island was located at $x = 15$ m and $y = 13$ m. The surface of the island and the floor of the basin were smooth by finished concrete. A directional spectral wave generator (DSWG) was installed along the x -axis and was used to generate solitary waves. The total length of the wave maker is 27.432 m and it consists of 60 individual paddles moving parallel to the water surface; each of them is independently and electronically driven. A sketch of the island geometry is also shown in Fig. 1 (Liu et al., 1995).

In laboratory experiments, four DWSG lengths, λ , were employed to generate incident solitary waves with different crest lengths. These are $\lambda = 6.401$, 13.259, 20.117 and 27.432 m. The nonlinearity of the incident solitary wave is defined with the height-to-depth ratio of the incident solitary wave, defined as $\varepsilon = A/h$ where h is the still-water depth. In experiments the constant water depth was fixed as $h = 0.32$ m and three different targets of initial solitary wave profiles were used with $A/h = 0.05$, 0.1 and 0.2, where A is the wave height of the incident solitary wave. In this paper, the study is focused on the case of $\varepsilon = 0.1$. Incident waves radiate in the horizontal direction before they reach the island and form a non-uniform crest line. The geometry of island in the basin system is symmetrical with respect to the line passing through the island center and perpendicular to the crests of incident waves. Time histories of free surface displacements were measured at 27 different locations. Locations of wave gages are plotted in Fig. 2. And the wave gages were installed around the island with an interval of $\pi/8$ so that we could measure the maximum run-up heights around a circular island.

More detailed description on laboratory experiments including facilities can be found in Liu et al. (1995), hence that is not repeated here again.

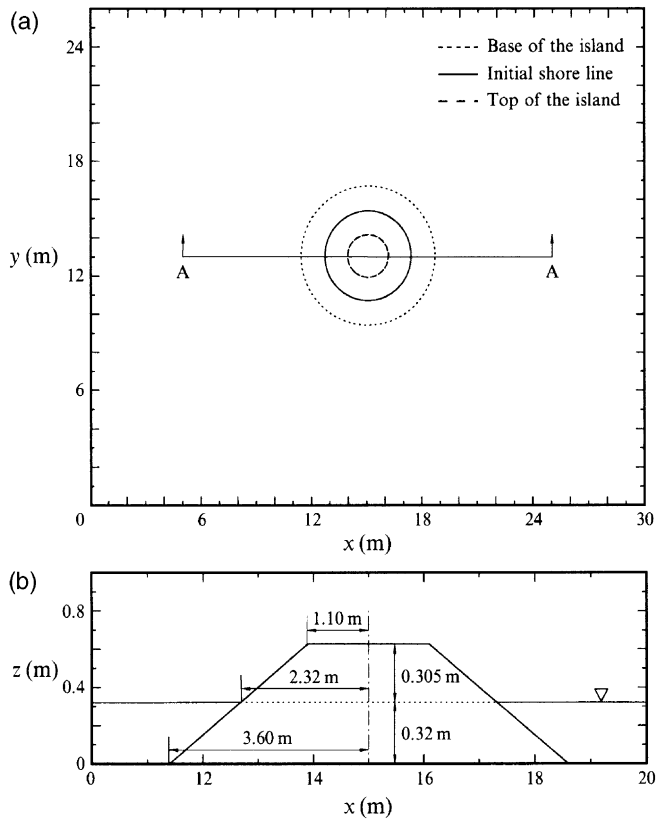


Fig. 1. Top view of the wave basin with the island and the vertical view of the circular island on the cross-section A-A.

3. Quadtree grid generation

Quadtree techniques were used for image processing by Samet (1982). Quadtree grids are robust to compute, cheap to produce and easy to adapt. Although they are not exactly boundary-fitting, quadtree grids can nearly approach the boundary with the use of high resolution boundary cells.

In order to generate a quadtree grid system, the domain of interest is normalized to fit within a unit square firstly. Then, the square is subdivided into four quadrants of equal size. Next subdivision of the square into subpanels carries out recursively about the seeding points. This involves checking each new panel in turn and subdividing if more than a prescribed minimum number of seeding points are found in the panel. A 2:1 ratio grid regularization is carried out whereby each cell is checked in order and subdivided if adjacent to a cell that is more than one level smaller. This regulation can reduce the number of cell configurations. Quadtree

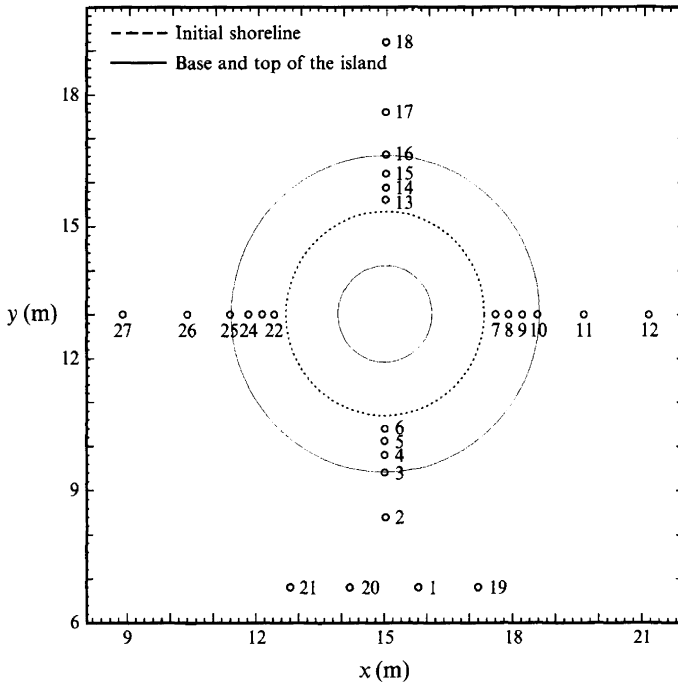


Fig. 2. Locations of free surface displacement gage stations.

adaptation is achieved straightforward using grid enrichment and coarsening by additional square subdivision (Park and Borthwick, 2001).

The tree structure of the quadtree is very helpful for cell identification, and neighbor finding by traversal. For the applications described in this paper, information on the quadtree grid is held using a linked list with memory pointers. Each link is built with pointers from the object cell to its parent cell and its subdivided cells. Hence, every cell is identified by knowing the tree path relative to the root (Park, 1999).

A systematic search of the tree reveals each cell and its neighbors by means of the nearest common ancestor (NCA); which is the smallest branching cell that is shared by the object cell and the neighbor under construction. Fig. 3 depicts a typical quadtree grid generated about seeding points. The associated hierarchical tree structure is illustrated in Fig. 4.

After the first stage of grid generation, the resulting grid often contains adjacent cells of different sizes with hanging nodes at the interface edges. A hanging node occurs where the vertex of one cell coincides with an edge of a neighbor cell and adjacent cells are more than one level apart in the quadtree. It should be noted that care has to be taken to ensure that conservation requirements are not violated when applying numerical approximations to the governing partial differential equations at hanging nodes.

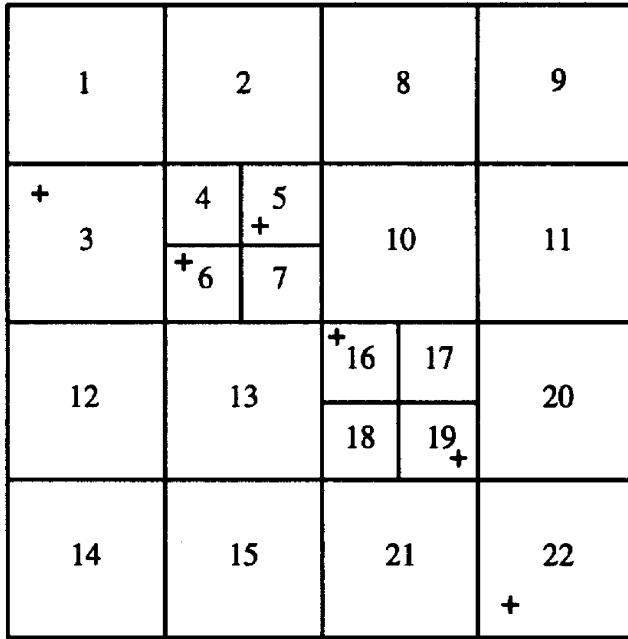


Fig. 3. Simple quadtree grid.

The following example shows the capability of the quadtree mesh generator to produce a Cartesian-type grid about a circle of 10,000 seeding points of radius 0.3 centered within the unit square. Fig. 5 depicts the quadtree grid of maximum level 8 obtained after 2:1 regularization has been applied. The grid contains 31,096 panels and 44,805 vertices.

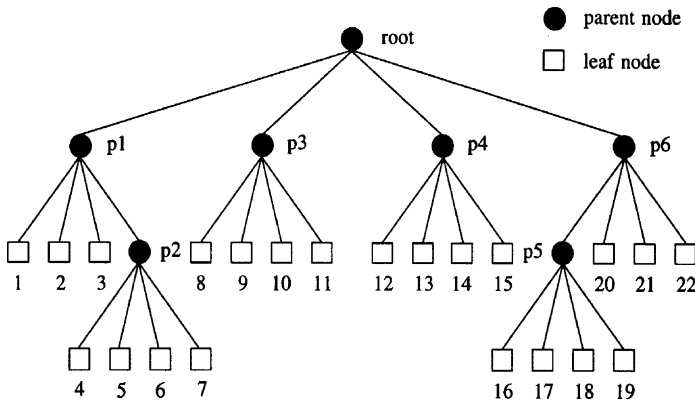


Fig. 4. Tree structure associated with Fig. 3.

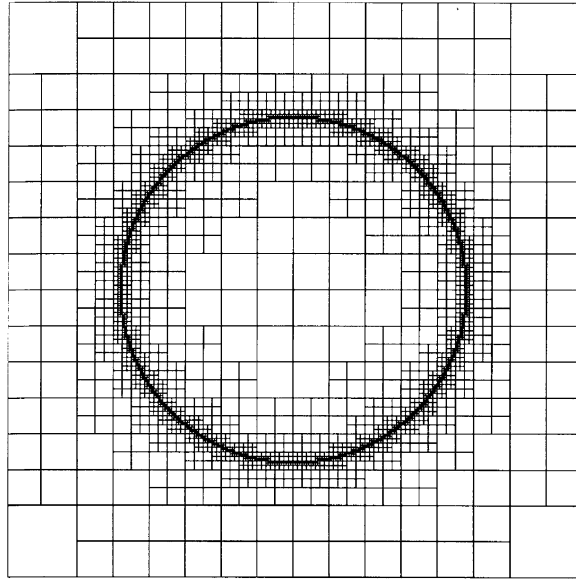


Fig. 5. An example of 8-level quadtree grid generated about a circle.

4. Governing equations and numerical model

As the tsunami approaches a coastal area, the wavelength of the incident tsunami becomes shorter and the amplitude becomes larger as the leading wave of a tsunami propagates into shallower water. Therefore, the nonlinear convective inertia force and bottom friction terms become increasingly important, while the significance of the Coriolis force and the frequency dispersion terms diminishes. The nonlinear shallow-water equations including bottom frictional effects are adequate to describe the flow motion in the coastal zone (Kajiura and Shuto, 1990; Liu et al., 1994). The nonlinear shallow-water equations on the staggered quadtree grids are shown as follows:

$$\frac{\partial \zeta}{\partial t} + \frac{\partial P}{\partial x} + \frac{\partial Q}{\partial y} = 0 \tag{1}$$

$$\frac{\partial P}{\partial t} + \frac{\partial}{\partial x} \left(\frac{P^2}{H} \right) + \frac{\partial}{\partial y} \left(\frac{PQ}{H} \right) + gH \frac{\partial \zeta}{\partial x} + \tau_x H = 0 \tag{2}$$

$$\frac{\partial Q}{\partial t} + \frac{\partial}{\partial x} \left(\frac{PQ}{H} \right) + \frac{\partial}{\partial y} \left(\frac{Q^2}{H} \right) + gH \frac{\partial \zeta}{\partial y} + \tau_y H = 0 \tag{3}$$

where ζ , the free surface displacements, P , the horizontal components of the volume flux in the x -direction, Q , the horizontal components of the volume flux in the y -direction and H , the total water depth (still-water depth + free surface displacement). Bottom friction terms can be modeled by using Manning’s formula,

i.e., $\tau_x = gn^2/H^{10/3}P(P^2 + Q^2)^{1/2}$, $\tau_y = gn^2/H^{10/3}Q(P^2 + Q^2)^{1/2}$ where n is the Manning’s relative roughness coefficient.

A staggered explicit finite difference leap-frog scheme is used to solve the governing equations, and nonlinear convective terms are linearized with an upwind scheme (Liu et al., 1995).

As shown in Fig. 6, the free surface displacement, ζ , and water depth, h , are defined at the center of each grid cell, while the volume flux components, P and Q , are defined at the interfaces of the grid. Numerical simulations of the laboratory experiments have been performed by Liu et al. (1995) in the uniform rectangular grids. Since the bottom frictional effect was found to be a small contribution to the maximum run-up heights around the island (Liu et al., 1995), it is not considered in the present study. The generation algorithm of solitary wave is given in Liu and Cho (1994).

In this paper, an adaptive quadtree grid system was employed to investigate the run-up height around a circular island. The refined quadtree grids were generated about a circular island with a rectangular and circular domain as shown in Fig. 7(a) and (b). By these methods, the numerical results were compared with laboratory experiments and it was determined that the quadtree model with a circular domain provided the most reasonable results. Consequently, only the quadtree model with a circular domain will be represented in this paper. A moving boundary treatment was implemented along the shoreline around the circular island, and radiation boundary conditions for outer boundaries are given by Liu et al. (1995).

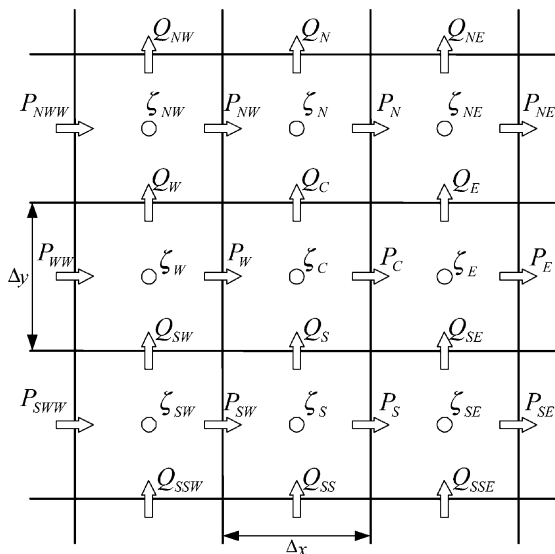


Fig. 6. Variables on staggered uniform quadtree grid.

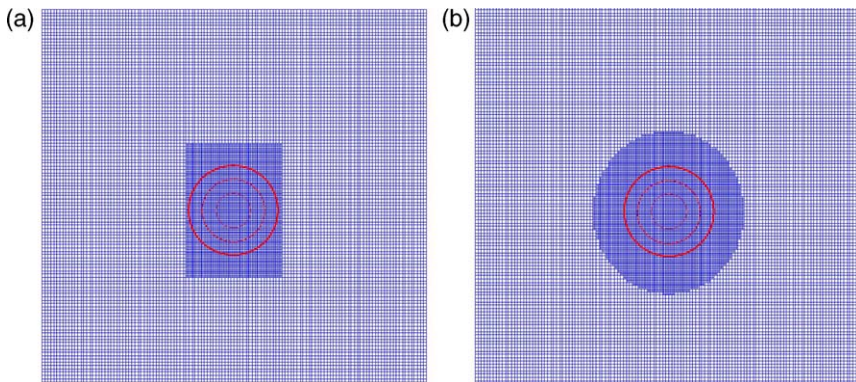


Fig. 7. (a) Rectangular domain; (b) circular domain.

5. Comparison and discussion

In order to verify the run-up heights of nearshore tsunami based on quadtree grids, comparisons are made with experimental measurements of the run-up heights on the circular island at the CERC. This section presents only a small portion of detailed numerical experiments (Liu et al., 1995).

5.1. Free surface displacements

To facilitate discussion of the results in the following sections, a sequence of snapshot-type figures of free surface displacements of an $\varepsilon = 0.1$ wave in vicinity of the circular island is first presented. In the numerical computations, time-step size was fixed as 0.02 s.

Fig. 8(a–c) presents snapshots of the free surface profiles at different times of 27.432 m DWSG length wave computed by the quadtree grids with a circular domain. As shown in Fig. 8(a), the incident solitary wave attacks the front end of the island and generates significant run-up. A portion of the wave propagates along the shoreline toward the lee side of the island (see Fig. 8(b), $t = 11$ s). Because of the island bathymetry, the crest line of the leading wave is bent, i.e., the wave form propagates with a faster speed offshore because of greater depth. Two wave components, the incident solitary wave and the trapped wave propagating around the island, are eventually separated at $t = 13$ s (see Fig. 8(c)).

At this moment, two trapped waves collide with each other in the lee side of the island and generate high run-up heights. Because they are not perfectly trapped, waves and certain amounts of energy are leaking continuously into offshore area. Then these trapped waves die out gradually.

Fig. 9 presents comparisons between wave gage data and numerical results about the uniform rectangular mesh (Liu et al., 1995). The quadtree grid system with a circular domain for an $\varepsilon = 0.1$ incident solitary wave and where the length of the wave generator is 27.432 m. Locations of the wave gages are shown in Fig. 2.

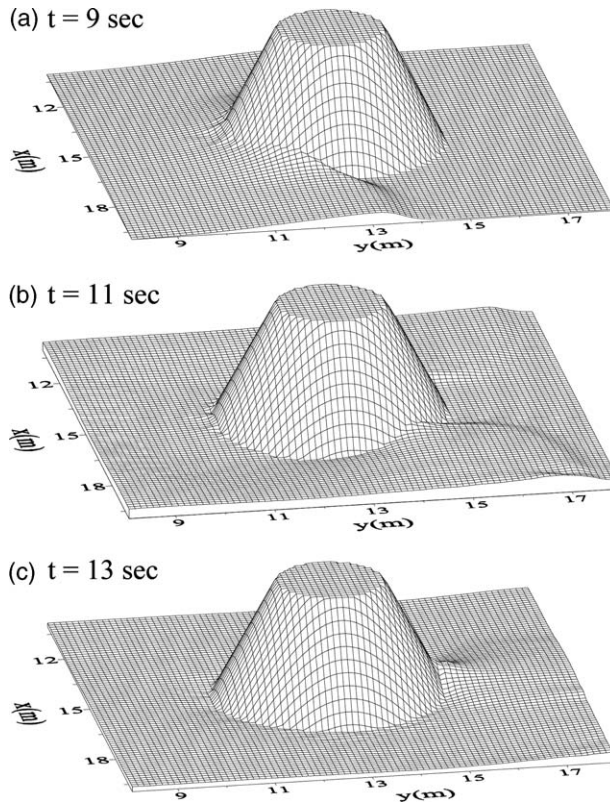


Fig. 8. (a–c) Snapshots of the free surface profiles using quadtree grids on circular domain ($\varepsilon = 0.1$, $\lambda = 27.432$ m).

Leading waves of numerical solutions are slightly stronger than frequency dispersion effects (Goring, 1978). Note that the second elevation wave appears in the experimental data, which cannot be reproduced in numerical solutions. This second elevation wave is re-reflected wave from the wave generator. In the numerical models, a radiation boundary condition has been employed so that the reflected wave from the island propagates out of the computational domains without being re-reflected.

On the lee side of the island the reflection of the solitary waves from the boundary of the basin is also evident (Fig. 9(g–l)). Once again, numerical results do not reproduce these reflected waves, because of the radiation boundary condition. However, these re-reflected waves do not affect the maximum run-up heights observed in the laboratory; the maximum run-up observed was always due to the first wave, and subsequent reflections produced significantly smaller run-up values (Liu et al., 1995).

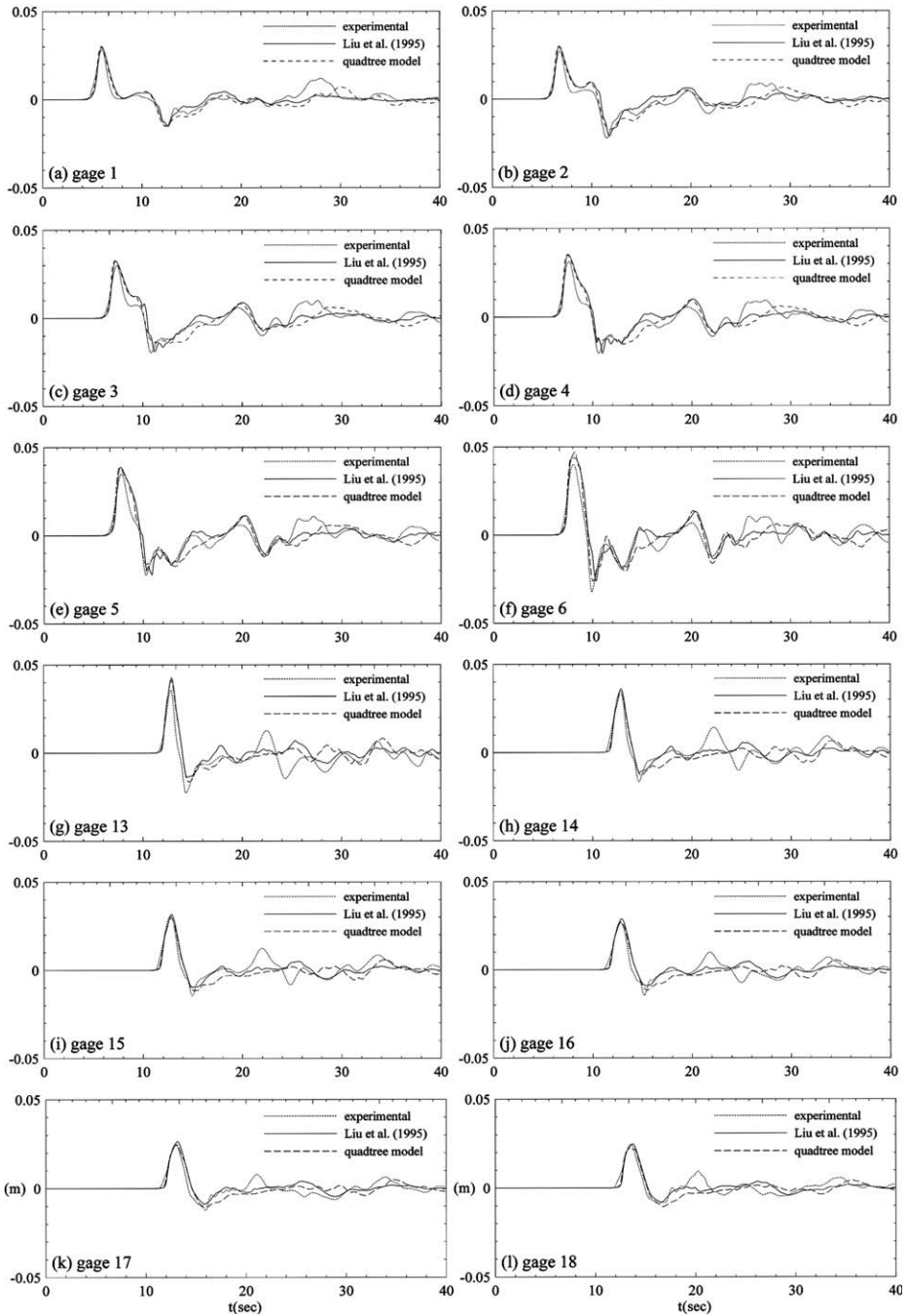


Fig. 9. (a–l) Time histories of free surface displacements ($\varepsilon = 0.1$, $\lambda = 27.432$ m) at different wave gage locations.

Although some re-reflections are observed, overall agreement between experimental data and the numerical solutions is good. The phase of free surface displacements analyzed by quadtree grids is in reasonable agreement against the results of uniform rectangular mesh.

5.2. Maximum run-up heights

In Fig. 10, normalized maximum run-up heights (R/A) around the island are presented for different incident wave crest length in case of $\varepsilon = 0.1$; where R is the run-up height and the angle β is measured in the counterclockwise direction around the island from the incoming wave direction with an interval of $\pi/8$ around the island.

Cho and Liu (1999) have investigated the effects of crest lengths of tsunamis on the maximum run-up heights. It has been found that the run-up heights around a circular island are strongly dependent on the crest length of incident waves, λ , when the crest length is less than the base diameter of the island but are almost insensitive if the crest length is greater than twice the base diameter D ; $D = 7.2$ m in this island.

In general, maximum run-up height is largest in front of the island (i.e. $\beta = 0$) and it decreases gradually as the wave moves toward the lee side of the island at $\beta = \pi$. If the length of the wave generator is much larger than the base diameter of the island (e.g. for $\lambda = 27.432$ m case), there is drastic increase in maximum run-up height at the lee side of the island, see for example, the $\beta = \pi$ case in Fig. 10(d). This is because the run-up heights in the lee are enhanced by the collision of the two propagating waves along the shelf of the island, to which the incident wave splits as shown in Fig. 8(c) (Liu et al., 1995).

In Fig. 10, the maximum run-up height increase as m increases. In other word, a longer source produces a higher run-up height and a small island is more vulnerable to tsunami attack than a large island. In general, the maximum run-up height is the largest at the front of the island except for two experiments ($\lambda = 20.117$ and 27.432 m). In these two experiments, maximum run-up heights observed in the lee of the island were slightly larger than those of the front. However, this feature does not appear in numerical solutions. This underestimation is probably due to artificial viscous effects of the upwind scheme used for the discretization of nonlinear convective terms of the momentum equations (Cho, 1995).

The agreement between experimental data and the numerical solutions by quadtree model is good except in the lee side of the island for $\lambda = 20.117$ m and 27.432 m as shown in Fig. 10. The run-up heights calculated by quadtree grids on circular domain show the best results in comparison with the experimental data. The reason is that the circular domain is concentrated on the island and the phases of the run-up are better represented along the shoreline.

The numerical model can calculate volume flux components, P and Q , for each time-step, which can be converted to the depth-averaged velocity vector. Fig. 11 shows a sequence of snapshots of velocity distributions at the back of the island, $\pi/2 < \beta < \pi$, for $\varepsilon = 0.1$ and $\lambda = 27.432$ m. Owing to symmetry, velocity patterns

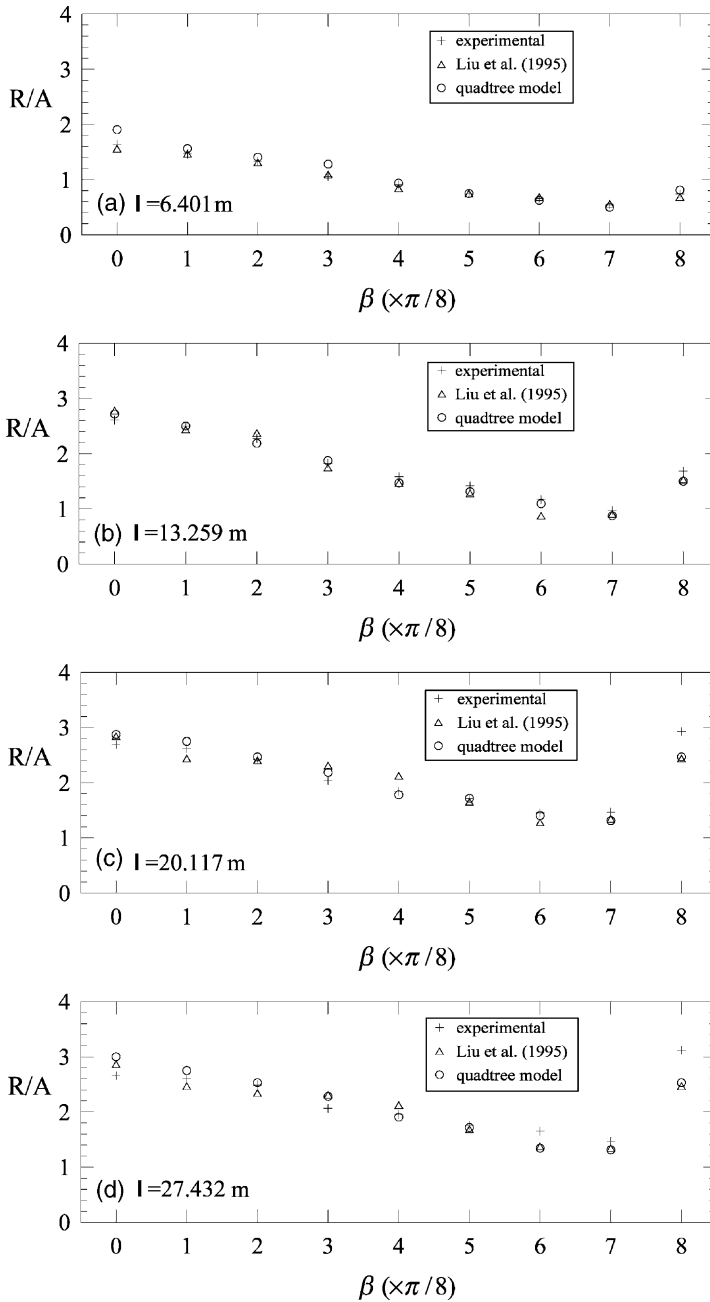


Fig. 10. (a–d) Comparisons of the normalized run-up height distribution around the island ($\varepsilon = 0.1$).

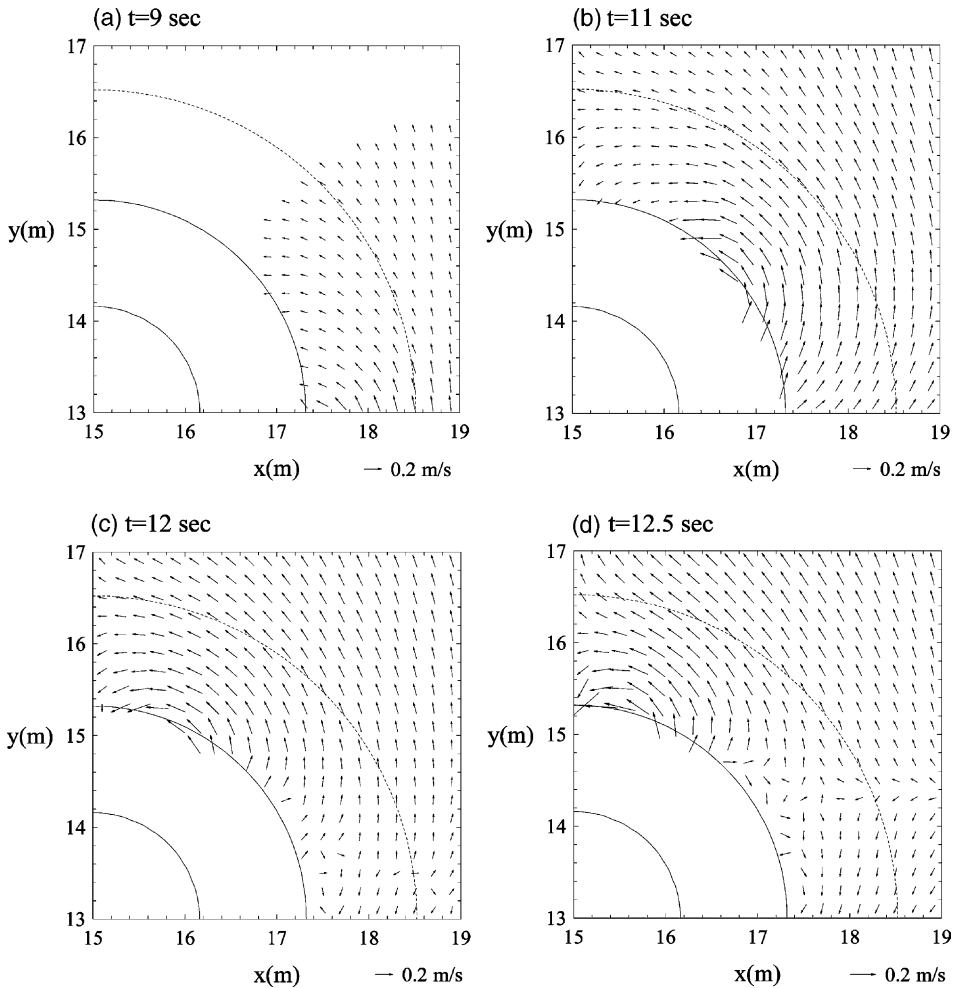


Fig. 11. (a–d) Snapshots of velocity distribution at the back of the island using quadtree grids on circular domain ($\varepsilon = 0.1$, $\lambda = 27.432$ m).

in the region $\pi < \beta < 3\pi/2$ are mirror images of those shown in Fig. 11. It is evident that although wave celerity is smaller near the shoreline, the depth-averaged particle velocity is much larger near the shoreline. Two trapped waves collide at the lee side of the island and create the maximum particle velocity at $t = 12.5$ s.

The affected area during the run-up in front of the island is much wider than that in the lee side of the island. In Fig. 12, a sequence of shoreline locations in front of the island before the run-up height reaches its maximum is shown. At the maximum run-up (i.e. $t = 9$ s), the entire front half of the island is inundated, while the run-up in the lee side of the island causes a much smaller inundated area (see Fig. 13). The difference can be explained as follows: during the run-up phase,

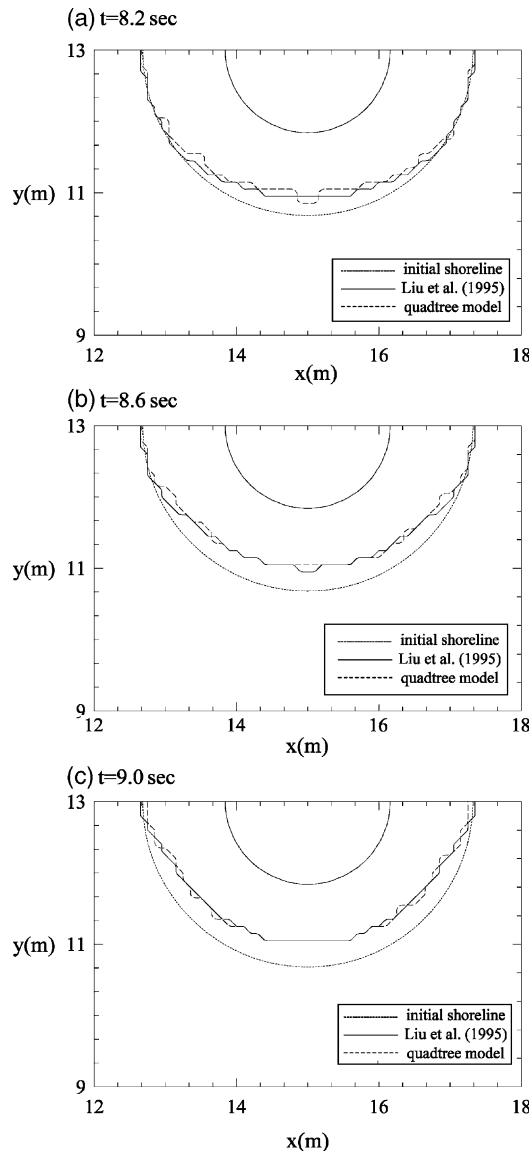


Fig. 12. (a–c) Instantaneous shoreline location in front of the island near the maximum run-up height for $\varepsilon = 0.1$ and $\lambda = 27.432$ m.

the velocity field in front of the island is mostly in the onshore direction over a relatively broad area. On the other hand, in the lee side of the island, the velocities are in the alongshore direction before the trapped waves collide with each other (see Fig. 11(c and d)). Because the shoreline is allowed to move, alongshore velocities near the shoreline turn into the onshore direction very sharply at the time

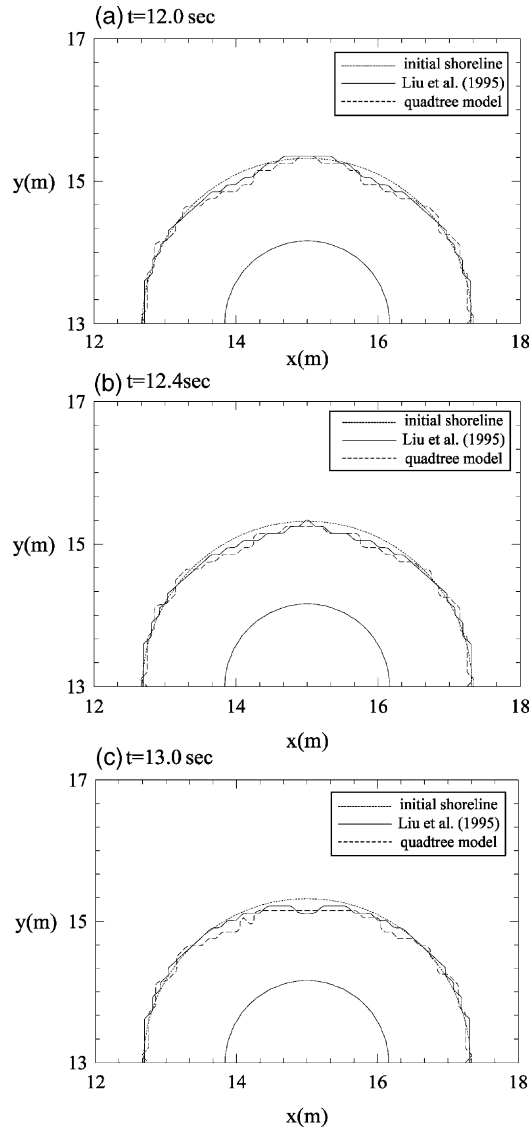


Fig. 13. (a–c) Instantaneous shoreline location in the lee side of the island near the maximum run-up height for $\varepsilon = 0.1$ and $\lambda = 27.432$ m.

of collision (Liu et al., 1995). This causes the enhanced and focused run-up area in the lee side of the island.

As shown in Figs. 12 and 13, the shorelines represented by quadtree domains show more practical appearances; on the other hand, the shorelines of uniform rectangular meshes are usually made of straight lines.

6. Concluding remarks

The numerical model is based on the shallow-water equations, developed by Liu et al. (1995), has been applied on the quadtree grids of the rectangular and circular domains for evaluation of run-up around a circular island. The results have been compared with laboratory data. It should be noted that when the laboratory manifestation of the wave does not break in the front of the island, the results have better agreement between laboratory data and numerical results by quadtree grid system than by uniform rectangular mesh.

The numerical scheme introduced in this study can be applied to forecast the maximum run-up heights on circular-shaped islands for possible tsunami attacks for more realistic results using quadtree grids which are straightforward to generate automatically, and also they can be locally refined according to the flow features.

Acknowledgements

The research was financially supported by the Meteorological Research Institute of the Korea Meteorological Administration.

References

- Cho, Y.-S., 1995. Numerical simulations of tsunami propagation and run-up. Ph.D. Thesis, Cornell University.
- Cho, Y.-S., Liu, P.L.-F., 1999. Crest length effects in nearshore tsunami run-up around islands. *J. Geophys. Res.* 104, 7907–7913.
- Gonzalez, F.I., 1999. Tsunami. *Sci. Am.* May, 56–65.
- Goring, D.G., 1978. Tsunamis—the Propagation of Long Waves onto a Shelf. W.M. Keck Laboratory of Hydraulics and Water Resource. California Institute of Technology, Rep. No. KH-R-38, pp. 310.
- Kajiura, K., Shuto, N., 1990. Tsunami. In: Le Mehaute, B., Hanes, D.M. (Eds.), *The Sea*. John Wiley, New York, pp. 395–420.
- Liu, P.L.-F., Cho, Y.-S., 1994. An integral equation model for wave propagation with bottom frictions. *J. Waterw. Port, Coastal Ocean Eng.* 120, 594–608.
- Liu, P.L.-F., Cho, Y.-S., Yoon, S.B., Seo, S.N., 1994. Numerical simulations of the 1960 Chilean tsunami propagation and inundation at Hilo, Hawaii. In: El-Sabh, M.I. (Ed.), *Recent Development in Tsunami Research*. Kluwer Academic Publishers.
- Liu, P.L.-F., Cho, Y.-S., Briggs, M.J., Kanoglu, U., Synolakis, C.E., 1995. Run-up of solitary wave on a circular island. *J. Fluid Mech.* 302, 259–285.
- Park, K.-Y., 1999. Quadtree grid numerical model of nearshore wave-current interaction. Ph.D. Thesis, Oxford University.
- Park, K.-Y., Borthwick, A.G.L., 2001. Quadtree grid numerical model of nearshore wave-current interaction. *Coastal Eng.* 42, 219–239.
- Pelinovsky, E., Troshina, E., Golinko, V., Osipenko, N., Petrukhin, N., 1999. Runup of tsunami waves on a vertical wall in a basin of complex topography. *Phys. Chem. Earth (B)* 214 (5), 431–436.
- Samet, H., 1982. Neighbour finding techniques for images represented by quadtrees. *Data Struct. Comput. Graphics Image Process.* 18, 37–57.
- Silva, R., Losada, I.J., Losada, M.A., 2000. Reflection and transmission of tsunami waves by coastal structures. *Appl. Ocean Res.* 22, 215–223.